



Heterogeneous activation of persulfate by reduced graphene oxide–elemental silver/magnetite nanohybrids for the oxidative degradation of pharmaceuticals and endocrine disrupting compounds in water



Chang Min Park^{a,b}, Jiyong Heo^c, Dengjun Wang^b, Chunming Su^{d,*}, Yeomin Yoon^{e,*}

^a Department of Environmental Engineering, Kyungpook National University, 80 Daehak-ro, Buk-gu, Daegu, 41566, South Korea

^b National Research Council Research Associate at the U.S. Environmental Protection Agency, 919 Kerr Research Drive, Ada, OK 74820, USA

^c Department of Civil and Environmental Engineering, Korea Army Academy at Youngcheon, 495 Hogook-ro, Gokyungneon, Youngcheon, Gyeongbuk 38900, South Korea

^d Groundwater, Watershed and Ecosystem Restoration Division, National Risk Management Research Laboratory, Office of Research and Development, U.S. Environmental Protection Agency, 919 Kerr Research Drive, Ada, OK 74820, USA

^e Department of Civil and Environmental Engineering, University of South Carolina, 300 Main Street, Columbia, SC 29208, USA

ARTICLE INFO

Keywords:
Heterogeneous activation
Peroxysulfate
Nanohybrid
Phenol
Sulfate radicals

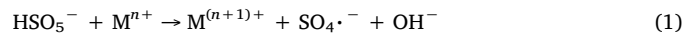
ABSTRACT

Reduced graphene oxide hybridized with zero-valent silver and magnetite nanoparticles (NPs) (rGO-Ag⁰/Fe₃O₄ nanohybrids) prepared via *in situ* nucleation and crystallization was used to activate peroxydisulfate (PDS) for degradation of pharmaceuticals and endocrine disrupting compounds (phenol, acetaminophen, ibuprofen, naproxen, bisphenol A, 17 β -estradiol, and 17 α -ethinyl estradiol). The deposition of Ag⁰ and Fe₃O₄ in rGO nanosheet enhanced the catalytic removal of phenol in the heterogeneous activation of PDS. The adsorption capacities of rGO-Ag⁰/Fe₃O₄ for 10 μ M phenol were 1.76, 1.33, and 2.04 μ mol g⁻¹-adsorbent at pH 4, 7, and 10, respectively, which are much higher than those of single NPs studied (Ag⁰, nanoscale zero-valent iron, and rGO). The rGO-Ag⁰/Fe₃O₄ effectively activated PDS to produce strong oxidizing SO₄²⁻ and facilitate an electron transfer on the surface of the nanohybrid. The initial pseudo-first-order rate (k_{ini}) constant for phenol degradation in PDS/rGO-Ag⁰/Fe₃O₄ system was 0.46 h⁻¹ at pH 7, which is approximately eight times higher than that in the presence of single NPs ($k_{\text{ini}} = 0.04\text{--}0.06\text{ h}^{-1}$) due to the synergistic effects between adsorption and catalytic oxidation. Among various organic contaminants tested, the simultaneous use of rGO-Ag⁰/Fe₃O₄ (0.1 g/L) and PDS (1 mM) achieved more than 99% degradation of acetaminophen and 17 β -estradiol at pH 7. The radical scavenging studies with methanol and natural organic matter indicated that phenol was more likely to be degraded via free SO₄²⁻ and \cdot OH formation or a non-radical oxidative pathway. Our findings indicate that the rGO-Ag⁰/Fe₃O₄ nanohybrids can be used as an efficient magnetically-separable nanocatalyst for removal of organic compounds in water and wastewater treatment.

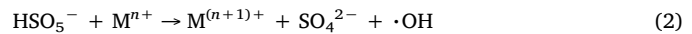
1. Introduction

Sulfate radical (SO₄²⁻, redox potential of 2.5–3.1 V), a strong one-electron oxidant, has attracted increasing attention due to its high efficiency and selectivity for the catalytic degradation of refractory organic contaminants and algal toxins (phenol, benzoic acid, 4-chlorophenol, and microcystin-LR) [1–4]. Generally, SO₄²⁻-precursors, persulfate (PS) (i.e., peroxymonosulfate (PMS, SO₅²⁻) or peroxydisulfate (PDS, S₂O₈²⁻)) can be activated effectively by external energy (e.g., heat [5], ultraviolet (UV) [6], ultrasound [7], and radiolysis [8]) or transition metal catalysts (i.e., Mⁿ⁺ = Ag(I), Ce(III), Co(II), Fe(II), Fe(III), Mn(II), Ni(II), Ru(III), and V(III)) [9] to produce SO₄²⁻ in a photochemical, thermal, or chemical processes. The transition metals

require much less energy and consumable chemicals for SO₄²⁻ generation compared with those using different energy activators [9]. For example, PMS can be activated by transition metals via the following two pathways (Eqs. (1) and (2)):



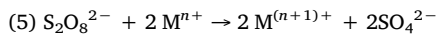
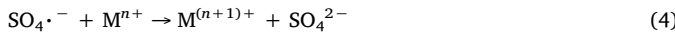
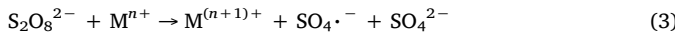
The hydroxyl radical (\cdot OH) may be formed during PMS activation, in Eq. (2):



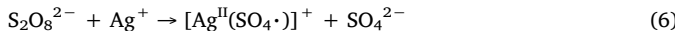
Similarly, SO₄²⁻ can be generated by transition metals via activation of PDS, as follows:

* Corresponding authors.

E-mail addresses: su.chunming@epa.gov (C. Su), yoony@cec.sc.edu (Y. Yoon).



A systematic study of several transition metal-PS/H₂O₂ couples for their reactivity toward degradation of a model organic substrate (2,4-dichlorophenol) showed that Ag(I) was the best activator for PDS in generating freely diffusible SO₄^{·-} (Eq. (3)), whereas Co(II) was the most effective for activating PMS [9]. It was also found that metal-bound (or caged) SO₄^{·-} may be produced with homogeneous Ag(I)/K₂S₂O₈ coupling reagent:



Although dissolved Ag(I)/Co(II) was highly effective in producing SO₄^{·-} in the activation of PS, the toxicity associated with dissolved metals is always a big concern in water and wastewater treatment. Alternatively, iron compounds (e.g., pyrite (FeS₂) [10], magnetite (Fe₃O₄) [11], core-shell Fe–Fe₂O₃ [12], or spinel-type ferrite (MFe₂O₄, M = Mn, Fe, Co, Ni, and Cu) [13]) have received great attention in a heterogeneous manner that immobilizes iron in support materials due to their excellent capabilities for PS activation and intrinsic magnetic properties, which facilitates easy phase-separation by simply using a magnet. However, excess feeding or sequential additions of Fe(II) can also play a role in quenching the formation of SO₄^{·-}, whereas Fe(II) is rapidly oxidized to Fe(III) (Eq. (4)). The zero-valent iron (ZVI, Fe⁰) can overcome these disadvantages by slowly releasing Fe(II) in water [14,15], but the rapid aggregation of ZVI induced by its magnetic property reduces the catalytic activity [16]. Carbon-based nanomaterials (CNMs) (e.g., carbon nanotubes [17,18] and graphene oxide (GO) [19–21]) have also been suggested as alternative catalysts as well as being excellent electron transfer mediators for organic compound oxidation in a heterogeneous PS activation system. Recently, the incorporation of metal/metal oxides nanoparticles (NPs) on CNMs has been explored as futuristic and cost-effective (photo)catalysts. Those nanohybrid (NH) materials are designed for synergistic effects between (photo)catalysis and the adsorption of organic contaminants or heavy metal ions [22]. Additionally, a lower aggregation propensity of NHs increases the overall specific surface area of the nano-catalysts, thus enhancing their performance in contaminant removal [23].

Among many CNMs, graphene and its derivatives have been used extensively to support metal/metal oxide NPs for the construction of graphene-based NHs due to their high electrical conductivity, chemical/mechanical stability, and large specific surface area and reactivity [24,25]. The hybridization of graphene with metal/metal oxide NPs can improve robustness against target contaminants and inhibit the corrosion/leaching of metal ions, which enhances the life span of the catalysts. Moreover, the delocalized π -electron systems of graphene renders a strong adsorption capacity for organic compounds by π - π stacking interactions [26]. There have been several attempts to improve the (photo)catalytic activity by controlling the composition of magnetic cobalt ferrite NPs [27] or combining graphene with various metal/metal oxides NPs. For example, Al-Anazi et al. [27] reported that the increase in molar ratio of cobalt in the spinel ferrite NPs (Co_xFe_{3-x}O₄; x = 0.1, 0.5, 0.7, 1.0) enhanced the degradation efficiency of 2-phenylbenzimidazole-5-sulfonic acid in activation of PMS into reactive SO₄^{·-} and ·OH without use of additional heat and light. P25, titanate nanotubes [28], ZnO [29], CuO [30]/Cu₂O [31], CuFe₂O₄ [32], and Bi₂WO₆ [33] have been assembled with graphene nanosheets as photocatalysts for organic dye removal. More recently, several facile approaches for synthesis of reduced graphene oxide (rGO)-based NHs with Mn₃O₄ [34], Co₃O₄ [35], Co(OH)₂ [36], MnFe₂O₄ [37], and CoFe₂O₄ [38] have been demonstrated to enhance the catalytic performance in heterogeneous activation of PMS system for degradation of organic dyes (e.g., methyl violet, methyl orange, methylene blue, orange II, and rhodamine B) or phenols. To our knowledge, there is no reported study

examining bimetallic rGO NH (silver and iron compounds deposited on a rGO nanosheet) as a heterogeneous PDS catalyst in degradation of organic contaminants, although those single metal/metal oxides have been found to be very efficient catalysts for SO₄^{·-} formation in PS activation systems.

Over the past few years, large groups of environmental contaminants such as pharmaceuticals and endocrine disrupting compounds (EDCs) have gained much attention because they are frequently detected at trace levels (< 0.1 $\mu\text{g/L}$) in surface water and wastewater [39–41]. Particularly, the pharmaceuticals and EDCs occurring in surface and ground waters are likely to have adverse impacts and potential risks to human health and ecology but are not commonly regulated [42]. In the current study, we tested the catalytic activity of rGO hybridized with zero-valent silver and magnetite (rGO-Ag⁰/Fe₃O₄) in the heterogeneous activation of PDS for the catalytic removal of phenol, acetaminophen, ibuprofen, naproxen, bisphenol A (BPA), 17 β -estradiol (E2), and 17 α -ethinyl estradiol (EE2). Specific objectives of this study were to provide the degradation efficiency of organic pollutants and insights into the mechanisms of phenol removal, including the possible involvement of reactive oxidizing species on the NH. The performance of rGO-Ag⁰/Fe₃O₄ was also compared with that of single (i.e., AgNP, nanoscale zero-valent iron (NZVI), and rGO) in the activation of H₂O₂. Our group recently synthesized the rGO-Ag⁰/Fe₃O₄ NH to investigate the aggregation kinetics and long-term stability under environmentally relevant conditions [43]. It was found that bimetallic rGO NH (rGO-Ag⁰/Fe₃O₄) showed excellent stability over a wide range of pH, type of electrolytes, and ionic strength (IS) conditions. We systematically characterized this highly stable NH and identified removal pathways for in-depth understanding of the mechanisms involved in the catalytic removal of organic compounds.

2. Experimental

2.1. Material preparation

A modified Hummers method was used to prepare GO [44]. The method involves the oxidative treatment of natural graphite flakes (3061 grade, Asbury Graphite Mills) with concentrated sulfuric acid and oxidizing agents followed by centrifugation, ultrasonication, washing, and separation via membrane filtration. A detailed description of the procedure is provided in the Supplementary Information. Phenol, acetaminophen, ibuprofen, naproxen, BPA, E2, and EE2 were purchased from Sigma-Aldrich Co. with purity higher than 98%. The physicochemical properties and chemical structures of the target organic compounds investigated are listed in Table S1. Suwannee River humic acid (SRHA, Standard II) and fulvic acid (SRFA, Standard II) were obtained from the International Humic Substances Society and were used as radical scavengers. Other chemicals used in this study (i.e., NaNO₃, KMnO₄, CH₃OH, Na₂S₂O₃, K₂S₂O₈, H₂O₂, H₂SO₄, HCl, and NaOH obtained from Sigma-Aldrich Co.) are of reagent grade. All solutions were prepared in ultra-pure water (> 18 MΩ/cm) obtained from a Milli-Q water purification system (Millipore Co.).

2.2. Characterization of rGO-based nanohybrids

The size and morphology of the synthesized rGO and rGO-Ag⁰/Fe₃O₄ NH were characterized by field-emission transmission electron microscopy (FE-TEM; Titan G2 with ChemiSTEM Cs Probe; FEI). X-ray photoelectron spectroscopy (XPS) of rGO and rGO-Ag⁰/Fe₃O₄ NH were obtained using a PHI Quantera SXM scanning X-ray microscope (ULVAC-PHI, Inc.). The structural properties of graphite, rGO, and rGO-Ag⁰/Fe₃O₄ NH were examined using a Rigaku Miniflex II X-ray diffractometer with Mn-filtered Fe K α radiation ($\lambda = 0.1937$ nm), operated at 30 kV and 15 mA. Powder X-ray diffraction (XRD) patterns were recorded from 20 of 2° to 90° in 0.02° step increments, and the peaks of the collected XRD patterns were analyzed with the software package,

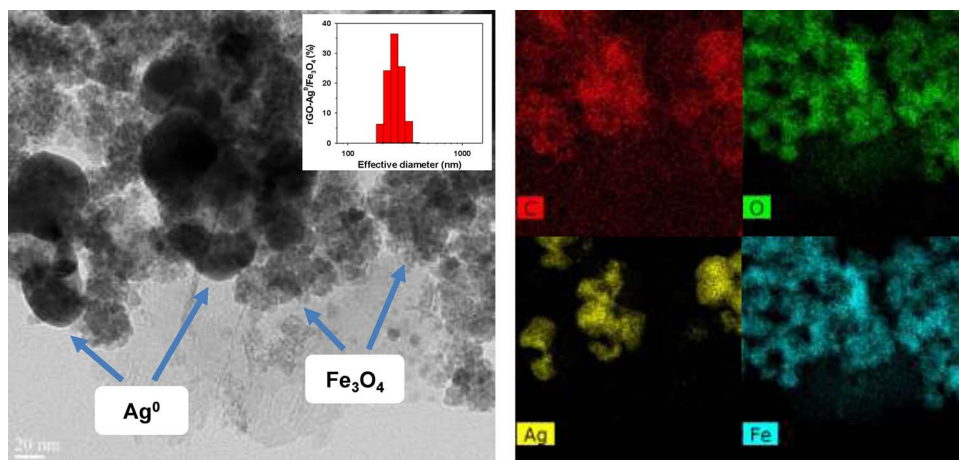


Fig. 1. FE-TEM micrograph, particle size distribution (inserted figure) of rGO-Ag⁰/Fe₃O₄ NH (left panel), and its elemental mapping results for C, O, Ag, and Fe (right panel).

Jade (Materials Data, Inc.) which allows data comparison with the JCPDS Powder Diffraction File database. The surface functional groups of rGO and rGO-Ag⁰/Fe₃O₄ NH were identified by Fourier transform-infrared (FT-IR) spectrometer (Thermo Scientific Nicolet 6700) in the wavenumber range of 400–4000 cm⁻¹. UV-vis spectra of AgNP (Sigma-Aldrich Inc.), rGO, and rGO-Ag⁰/Fe₃O₄ NH were recorded on a Lambda 35 UV-vis spectrophotometer (Perkin-Elmer) in the wavelength range of 200–900 nm.

2.3. Catalytic degradation experiments

The degradation experiments in heterogeneous activation of PDS and H₂O₂ were conducted in duplicate in 60 mL amber glass bottles containing 10 μM of phenol and other organic contaminants (*i.e.*, acetaminophen, ibuprofen, naproxen, BPA, E2, and EE2). The bottles were covered completely with aluminum foil to avoid potential photo-degradation during the reaction processes. To initiate the catalytic reaction, 1 mM PDS or H₂O₂ were added to the solution. At predetermined time intervals, 1 mL aliquot of the sample was withdrawn, and the reaction was immediately quenched by adding 0.5 M Na₂S₂O₃ solution to the mixture. The NPs were then removed by high-speed centrifugation (18,000g) for 15 min followed by filtration (0.45-μm filter membrane (VWR, USA). The filtrates were loaded on to a high-performance liquid chromatography (HPLC) system (Hewlett Packard, Agilent 1100) for all chromatographic analyses of organic compounds, which were measured using a C18 column (Zorbax Eclipse XDB-C18, 150 × 4.6 mm²; *i.d.* 5 μm) coupled to a compatible guard column with HPLC-grade mobile phase reagents (acetonitrile/methanol) and water at a flow rate of 0.5–1 mL/min. The UV-vis-diode array detector was set at 254 nm for acetaminophen and 210 nm for ibuprofen [45]. A HPLC-fluorescence detector method was used to detect phenol, naproxen, BPA, E2, and EE2. The initial degradation rate constants (k_{ini}) were calculated by a pseudo-first-order kinetic model for the first 1 h of reaction (Tables S2 and S3). The quenching experiments were also conducted to determine the radical (SO₄^{·-}) scavenging effects using methanol (100 mM), SRHA (10 mg/L), and SRFA (10 mg/L) in heterogeneous PDS/rGO-Ag⁰/Fe₃O₄ system.

2.4. Adsorption

Prior to the degradation reaction described above, batch kinetic experiments were carried out at 298 K to determine the kinetic parameters for the adsorption of phenol (10 μM) on the ultrasonically dispersed AgNP, NZVI (Nanoiron Inc.), rGO, and rGO-Ag⁰/Fe₃O₄ (0.1 g/L) at a sonication bath with an output of 70 W at a frequency of 42 kHz (Branson 1510 sonicator) for 30 min. The pH of the solution was adjusted to 4, 7, and 10 using 0.001–0.1 M HCl and NaOH solutions. A

small volume of samples was taken from the solution at predetermined time intervals with continuous stirring for 6 h, and then diluted 10 times to obtain a total volume of 10 mL. The supernatants were immediately centrifuged (18,000g) for 15 min and filtered through the 0.45-μm pore size filter membrane to remove residual particulates. Phenol concentration was determined by a HPLC system. The experiments were performed in triplicates.

3. Results and discussion

3.1. Properties of nanoparticles

The morphology and structures of rGO and rGO-Ag⁰/Fe₃O₄ NH were observed by FE-TEM. The elemental mapping results in Figs. 1 and S1 show that Ag⁰ and Fe₃O₄ NPs were deposited directly on the surfaces of rGO by *in situ* nucleation and crystallization; the diameters of Ag⁰ and Fe₃O₄ NPs were observed to be 50–200 nm. It can be clearly seen that the rGO layers of its NHs have several wrinkles due to extremely thin layers (~1 nm thick) [46,47]. The surface of rGO-Ag⁰/Fe₃O₄ NH showed a high degree of entanglement (fluffy sphere-like structure) but less aggregation (effective diameters of 220–300 nm than rGO (400–710 nm).

The crystal structures of rGO and rGO-Ag⁰/Fe₃O₄ NH were identified by their characteristic peaks in the XRD patterns (Fe K_α radiation; Fig. 2(a)). A strong diffraction peak of rGO with a *c*-axis interlayer spacing (*d*) of 3.45 Å at 32.6° (20) corresponds to the (002) crystalline plane of graphite (JCPDS No. 01-089-8487), indicating high crystallinity of the pristine graphite. XRD patterns of rGO-Ag⁰/Fe₃O₄ NH showed a relatively small diffraction peak of graphite centered at 33.1° (20; interlayer spacing of 3.40 Å), which may be ascribed to compressive loading of silver ions on rGO and a reduction effect [48]. Instead, three other crystalline phases of Ag⁰-3C, *syn* (JCPDS No. 01-087-0597) were observed for those NHs at 48.5, 56.6, and 84.1° (20) with *d* = 2.36, 2.04, and 1.44 Å, which, respectively, indexed as the (111), (200), and (220) faces. The rGO-Ag⁰/Fe₃O₄ NH showed a broad diffraction peak at 45.5° (20) with *d* = 2.50 Å, indexed to the (311) planes of magnetite crystal (Fe₃O₄, JCPDS No. 01-075-0449).

Variations in the surface functional groups of rGO and rGO-Ag⁰/Fe₃O₄ NH were analyzed via FT-IR spectroscopy (Fig. 2b). The strong peaks of rGO at 1402, 1173, and 877 cm⁻¹ corresponded to aliphatic C–H bending, C–O–C stretching, and aromatic C–H bending vibration, respectively. The sharp absorption peaks of rGO-Ag⁰/Fe₃O₄ NH at around 1633 and 1538 cm⁻¹ could be ascribed to the C=C and C=O stretching vibrations, respectively [49,50]. The weak peaks at 3300 and 2926 cm⁻¹ were assigned to O–H and C–H stretching vibrations. Many peaks in the fingerprint regions between 1600 and 660 cm⁻¹ for rGO moved to peaks around 1800–1100 cm⁻¹ for rGO-Ag⁰/Fe₃O₄ NH due to the deposition of Ag⁰ and Fe₃O₄ on rGO nanosheet.

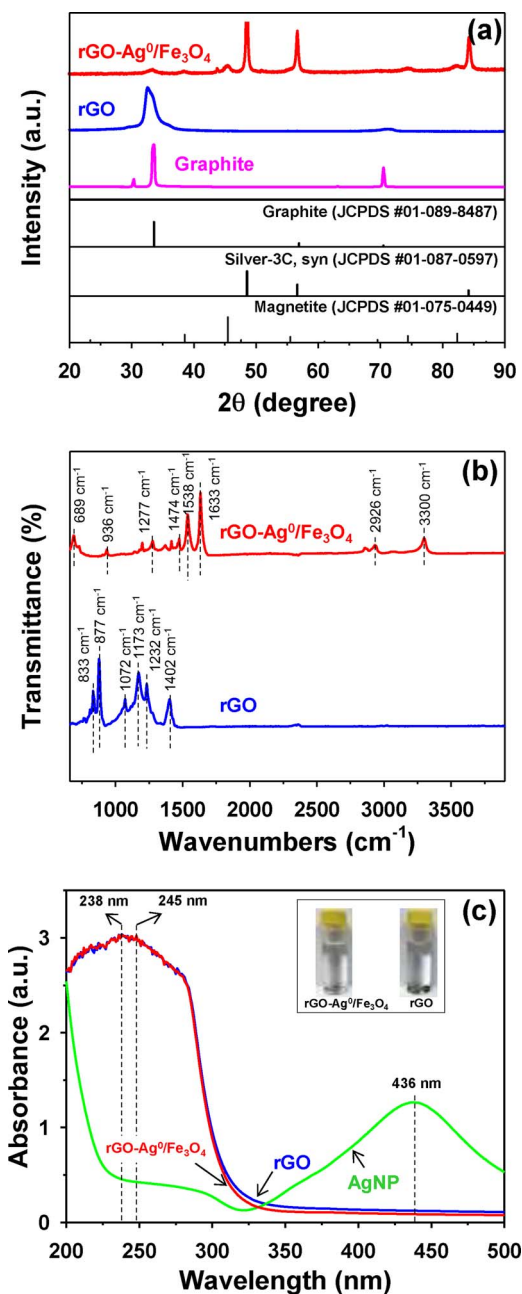


Fig. 2. (a) XRD patterns, (b) FT-IR spectra, and (c) UV-vis absorption spectra of rGO, AgNP, and rGO-Ag⁰/Fe₃O₄ NH.

Fig. 2c shows the UV-vis diffuse reflectance spectra of the AgNP, rGO, and rGO-Ag⁰/Fe₃O₄ NH. NZVI did not exhibit any obvious absorbance peak (data not shown) [51]. The surface plasmon resonance band of the Ag⁰ NPs was observed at 436 nm [52]. The absence of absorption peak of rGO-Ag⁰/Fe₃O₄ NH in the visible region indicates that Ag⁰ NPs are fully wrapped by the negatively charged rGO sheets, which also caused little shift in the maximum absorption peak position with a similar spectral shape of rGO by the deposition of Ag⁰ and Fe₃O₄ NPs (rGO-Ag⁰/Fe₃O₄ NH) on rGO.

XPS was used to confirm the chemical compositions of rGO and rGO-Ag⁰/Fe₃O₄ NH. A wide survey scan of C1 s and O1 s spectra was taken in the range of binding energy (BE), 0–800 eV (Fig. 3a). No extra peak was observed, ruling out any impurities other than C, O, Ag, and Fe elements. Table S2 shows C1 s and O1 s XPS curve fitting results of rGO and rGO-Ag⁰/Fe₃O₄ NH. The strong C1 s peak of rGO at 284.3 eV assigned to non-oxygenated (aromatic) carbon (C–C/C=C), decreased

appreciably, whereas peaks of rGO-Ag⁰/Fe₃O₄ NH at 286.1 and 288.8 eV, assigned to epoxy or hydroxyl carbon, C–O and carboxylate carbon, COO[–], respectively, arose when Ag⁰ and Fe₃O₄ NPs were deposited on rGO [53]. Other peaks at 287.0–287.8 eV correspond to carbons attached to different O-containing moiety, C=O. The deconvolution of the wide and asymmetric O1 s peak showed that a main peak of rGO (77.4%) at 532.2 eV was attributed to carbonyl and carboxyl oxygen (C=O). The weakest O1 s peak (1.45%) occurred at 530.0 eV, which was assigned to a quinone-type oxygen (COO[–]/C=O). The rGO-Ag⁰/Fe₃O₄ NH showed reduced O1 s peaks (21.4%) at 532.4 eV, but their O1 s peaks at 530.2 eV increased significantly to 49.0% [54]. These peak shifts, by 1.8–2.0 eV, towards lower BE indicated higher exposure to oxygen during the chemical reductive synthesis of NH. The notable peaks of rGO-Ag⁰/Fe₃O₄ at 368.2 and 374.2 eV in Ag3d region of high-resolution XPS curve (Fig. 3(d)) result from Ag 3d_{5/2} and Ag 3d_{3/2}, respectively due to a strong interaction of Ag core with the carboxyl oxygen (C=O) [55]. This result indicates that silver is deposited on rGO surface in metallic form (Ag⁰). The other two peaks centered at 367.4 and 368.8 eV reveal little contribution to AgO and Ag⁺, respectively. The main peaks of centered at 710.7–711.9 (including satellite peak at 718.2 eV) and 724.0 eV (including satellite peaks at 728.6 and 733.9 eV) in Fe2p region of XPS spectra (Fig. 3(e)) are expected to the binding energy of Fe2p_{3/2} and Fe2p_{1/2}, respectively, which corresponds to Fe³⁺ state of magnetite [56]. Overall, the deposition of Ag⁰ and Fe₃O₄ NPs on rGO sheet (rGO-Ag⁰/Fe₃O₄ NH) has enhanced surface reactivity and the surface site availability of NH due to the incorporation of the transition metals and reduced NP aggregation. In addition, the stronger peak (C–O) at 286.1 eV and lower C/O atomic ratio of NH may cause higher adsorption capacity via Lewis acid-base or π–π interaction.

3.2. Activation of PDS and H₂O₂ with rGO nanohybrid for phenol degradation

PDS or H₂O₂ alone was nonreactive towards phenol degradation during 6 h of reaction (Fig. S2). In Figs. 4 and S3, the activation efficiencies of PDS and H₂O₂ by the four NPs (i.e., AgNP, NZVI, rGO, and rGO-Ag⁰/Fe₃O₄) were compared for the catalytic degradation of phenol at pH 4, 7, and 10. The control experiments were also performed using the two single metallic rGO NPs (i.e., rGO-Ag⁰ and rGO-Fe₃O₄) with PDS and H₂O₂ (data not shown). In the presence of different NPs, when PDS or H₂O₂ was introduced in the heterogeneous activation systems, the decomposition of PDS or H₂O₂ occurred immediately either in the suspension or on the surface of NPs, although complete phenol removal was not achieved within 6 h (Figs. 4, S2, and S3). As water molecules ($E^{\circ}(\cdot\text{OH}/\text{H}_2\text{O}) = +2.80 \text{ V/NHE}$) cannot be oxidized thermodynamically by PDS/H₂O₂ alone ($E^{\circ}(\text{S}_2\text{O}_8^{2-}/\text{SO}_4^{2-}) = +2.01 \text{ V/NHE}$ and $E^{\circ}(\text{H}_2\text{O}_2/\text{H}_2\text{O}) = +1.78 \text{ V/NHE}$) [2], the catalytic reduction of PDS/H₂O₂ via direct one/two-electron transfer will only occur on the surface of highly reactive NPs.

Among the six NPs examined including control experiments, rGO-Ag⁰/Fe₃O₄ showed the highest removal efficiency towards phenol in the activation of PDS at all pH values. The k_{ini} values for rGO-Ag⁰/Fe₃O₄ at pH 4, 7, and 10 were 0.67, 0.46, and 0.23 h^{–1} in PDS and 0.10, 0.04, and 0.10 h^{–1} in H₂O₂, respectively. This is due to synergistic effect between higher adsorption of phenol (described below) and greater catalytic oxidation in activation of PDS than H₂O₂. In the catalytic activation of PDS and H₂O₂, the reaction rates of phenol removal under an acidic condition (pH 4) were higher than those under neutral and basic conditions (pH 7 and 10; Table S3). The less negative charge of NPs resulting from protonation of the hydroxyl groups under acidic condition (pH 4) will decrease the electrostatic repulsive force between PDS/H₂O₂ and the surface sites of NPs, promoting the removal of phenol in the suspension [57]. Liang and Su demonstrated, using a chemical probe method to thermal activation of PS, that SO₄^{2–} were dominant species under acidic conditions, whereas the amount of ·OH increased

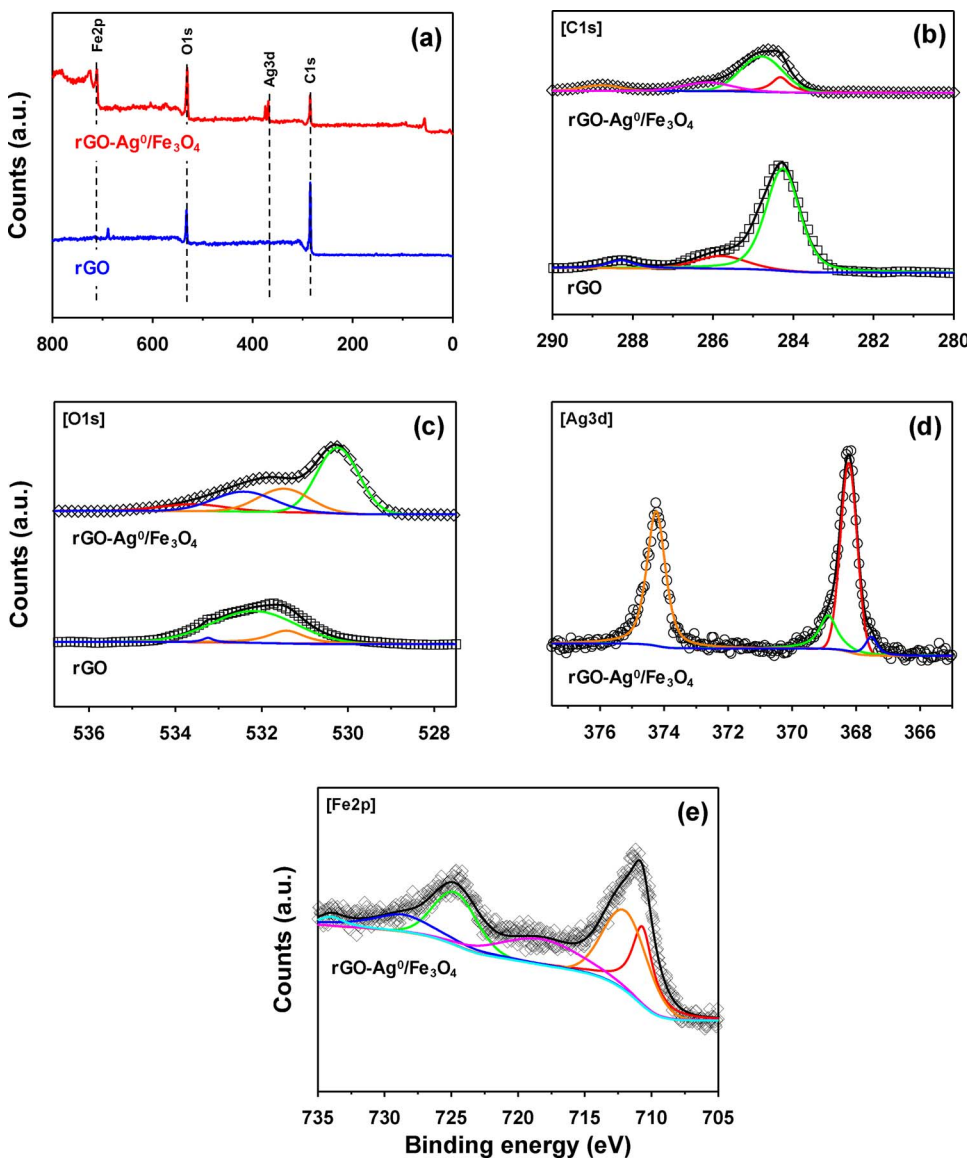


Fig. 3. X-ray photoelectron spectra of (a) wide survey scan and deconvolution, (b) C1s, (c) O1s, (d) Ag3d, and (e) Fe2p spectra of rGO and rGO-Ag⁰/Fe₃O₄ NH.

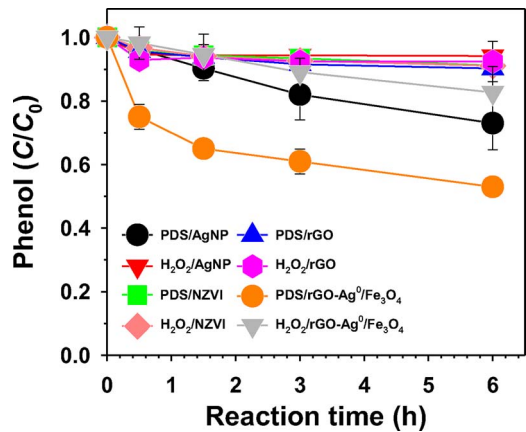
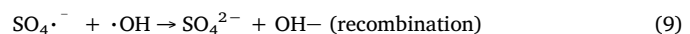
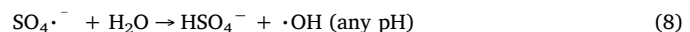
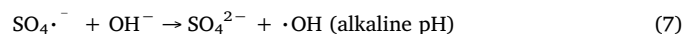


Fig. 4. Removal of phenol by AgNP, NZVI, rGO and rGO-Ag⁰/Fe₃O₄ NH in catalytic activation of PDS and H₂O₂. Experimental conditions: [AgNP]₀ = [NZVI]₀ = [rGO]₀ = [rGO-Ag⁰/Fe₃O₄]₀ = 0.1 g/L; [phenol]₀ = 10 μ M; [PDS]₀ = [H₂O₂]₀ = 1 mM; pH = 7; and temperature = 298 K.

to co-exist in the aqueous solution as the pH increased [58]. The SO₄^{·-} radical can be converted into the ·OH by undergoing reactions with hydroxyl OH⁻ ions in the alkaline pH range (Eq. (7)) or with water molecules at any pH value (Eq. (8)) [59]. The ·OH formed at higher pH acts as a SO₄^{·-} scavenger, to be reconverted to SO₄²⁻ ions (Eq. (9)), which will reduce the degradation rate of organic compounds under neutral/basic conditions in the PDS/rGO-Ag⁰/Fe₃O₄ system.



Thus, the reduced freely diffusible SO₄^{·-} at high pH will decrease the degradation efficiency of phenol. This suggests that the pH-dependent surface charge of NPs would likely determine the reactivity for the adsorption as well as degradation of phenol via a radical-mediated oxidation. It was also found that 47% of phenol was removed with a PDS/rGO-Ag⁰/Fe₃O₄ coupled process ($k_{\text{ini}} = 0.46 \text{ h}^{-1}$) at a neutral pH, whereas 17% was removed in the activation of H₂O₂ ($k_{\text{ini}} = 0.04 \text{ h}^{-1}$). These results indicate that SO₄^{·-} play a more important role in degradation of phenol than ·OH.

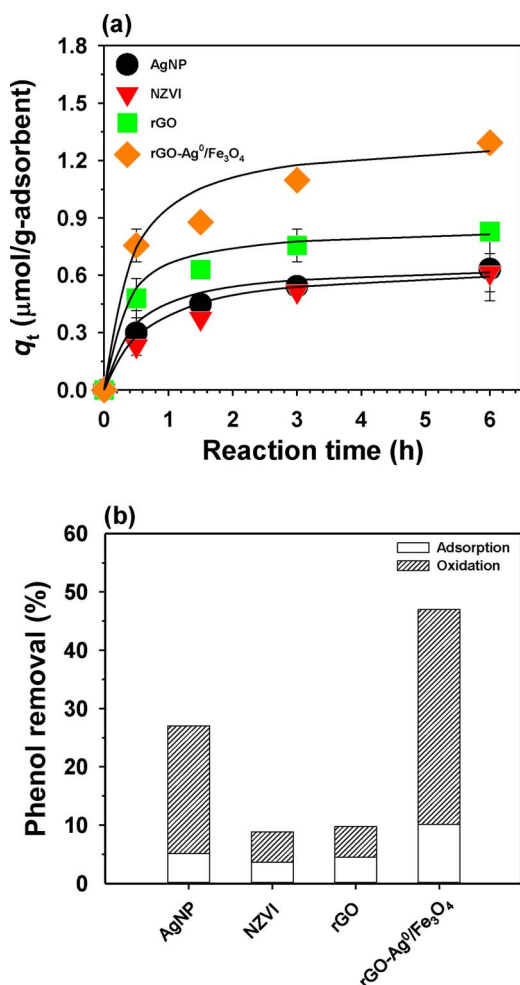


Fig. 5. (a) Adsorptive removal of phenol by AgNP, NZVI, rGO and rGO-Ag⁰/Fe₃O₄ NH. Solid lines are calculated from nonlinear least square regression of the adsorption data according to pseudo-second-order kinetic model. (b) Adsorptive removal and oxidative degradation of phenol after 6 h of reaction. The oxidation was only counted for the un-adsorbed fraction of phenol after 6 h of adsorption experiments. Experimental conditions: [AgNP]₀ = [NZVI]₀ = [rGO]₀ = [rGO-Ag⁰/Fe₃O₄]₀ = 0.1 g/L; [phenol]₀ = 10 μM; pH = 7; and temperature = 298 K.

3.3. Adsorption kinetics of phenol on rGO nanohybrid

To further quantify the role of the adsorption on the catalytic removal of phenol, phenol uptake by the four NPs was determined at pH 4, 7, and 10 prior to 6 h of degradation reaction (Figs. 5 and S4). The kinetic adsorption data were described using the pseudo-second-order kinetic model given in Eq. (10) [60,61], and the kinetics parameters of phenol adsorption are listed in Table S4.

$$\frac{dq_t}{dt} = k(q_e - q_t)^2 \quad (10)$$

which can be written as Eq. (11).

$$\frac{t}{q_t} = \frac{1}{kq_e^2} + \frac{t}{q_e} \quad (11)$$

where q_t and q_e ($= (C_0 - C_e)V/m$) are the amounts of phenol adsorbed at time t and at equilibrium state ($\mu\text{mol/g-adsorbent}$), k is the apparent adsorption rate constant ($\text{g-adsorbent}/\mu\text{mol h}$), V is the volume of suspension (L), and m is the mass of dry adsorbent (g). As shown in Figs. 5 a, S4a, and S4c, the adsorption capacity of NPs increased in the order of rGO-Ag⁰/Fe₃O₄ > rGO > NZVI \geq AgNP. The rGO-based NPs exhibited a higher adsorption efficiency of phenol than that of the other two NPs because of the unique property of rGO nanosheets (one-atom-

thick two-dimensional structure) with sp^2 hybridized carbon atoms, which facilitates direct contact with phenol via strong π - π interaction [62]. The rGO-Ag⁰/Fe₃O₄ NH showed at least 1.3 times higher adsorption efficiency of phenol than that of rGO (1.76, 1.33, and 2.04 $\mu\text{mol/g-adsorbent}$ for rGO-Ag⁰/Fe₃O₄ and 1.08, 0.86, and 1.51 $\mu\text{mol/g-adsorbent}$ for rGO at pH 4, 7, and 10, respectively), indicating that the hybridization with Ag⁰ and Fe₃O₄ on rGO increased the adsorption capacity. This also indicates that the higher adsorption capacity of rGO-Ag⁰/Fe₃O₄ toward phenol is not positively correlated to the π - π interaction because the degree of reduction of rGO was higher than rGO-Ag⁰/Fe₃O₄ (the atomic ratio of C/O = 4.8 for rGO and 1.3 for rGO-Ag⁰/Fe₃O₄ as confirmed by XPS analysis). It is instead attributed to the following two aspects: (i) the deposition of Ag⁰ and Fe₃O₄ on rGO nanosheets reduces the nanoparticle aggregation [43]; making more reactive surface sites available for phenol adsorption. Assembling magnetic iron oxide (e.g., magnetite) into rGO provides magnetic attraction, which promotes particle aggregation between rGO-Fe₃O₄ NPs [43]. However, the bimetallic rGO NH with zero-valent silver and magnetite showed smaller hydrodynamic sizes (D_h) over a wide range of pH, type of cations, and IEs due to a higher electrostatic repulsion by rGO NHs edge-edge interactions in the aquatic environment. (ii) the higher occupying epoxy or hydroxyl groups of rGO-Ag⁰/Fe₃O₄ (17.6%) than rGO (12.5%) can act as more Lewis base sites responsible for the formation of chemical bonding with phenolic hydroxyl group of phenol [53].

The total amount of phenol removed by the four NPs as well as the percentage of adsorption and oxidation were calculated in Table S5. There was a noticeable oxidation (85.4%), particularly under acidic conditions (pH 4), in the PDS/rGO-Ag⁰/Fe₃O₄ system following a higher amount of adsorption (14.6%) observed with rGO-Ag⁰/Fe₃O₄. Similarly, rGO-Ag⁰/Fe₃O₄ NH in catalytic activation of H₂O₂ exhibited greater oxidative degradation of phenol than that of single NPs under acidic/neutral conditions (pH 4 and 10), but the oxidation performance was much lower than PDS at all pH values tested. This confirmed that rGO-Ag⁰/Fe₃O₄ was responsible for enhanced activation of PDS on the surface of the NH (via non-radical oxidative pathway in which the organic compounds are oxidized by donating electrons to PDS/H₂O₂ on NPs) or in suspension to produce free SO₄²⁻ and ·OH. In contrast, NZVI is much stronger in activating H₂O₂ to form ·OH under acidic and neutral conditions (12.1 and 5.26% of phenol removal at pH 4 and 7, respectively) than PDS (6.04 and 5.21% at pH 4 and 7, respectively), whereas rGO was more active for H₂O₂ activation under acidic conditions (15.4% at pH 4) than PDS (12.8% at pH 4). This is the first study reporting the high efficiency of rGO-Ag⁰/Fe₃O₄ NH in the heterogeneous activation of PDS, promoting the catalytic oxidation of phenol. In this study, we also undertook further investigations of selectivity towards various organic compounds, degradation kinetics, and mechanisms for evaluating the potential of the PDS/rGO-Ag⁰/Fe₃O₄ system in the removal of organic pollutants.

3.4. Selectivity of the PDS/rGO-Ag⁰/Fe₃O₄ NH oxidation system

Fig. 6 shows the oxidative degradation kinetics of selected organic compounds (i.e., acetaminophen, ibuprofen, naproxen, BPA, E2, and EE2 (Table S1)) in the PDS/rGO-Ag⁰/Fe₃O₄ system. In contrast to low substrate-dependent reactivity under acidic conditions (pH 4), substrate specific-reactivity was evident under neutral/basic conditions (pH 7 and 10). Significant degradation (> 90% in 1 h of reaction) of acetaminophen, ibuprofen, E2, and EE2 and moderate degradation of naproxen and BPA (50–90% in 1 h reaction) were observed under acidic conditions (pH 4). However, ibuprofen and EE2 showed moderate degrees of degradation under neutral/basic conditions (pH 7 and 10), whereas a low level of degradation (< 50% in 1 h reaction) was observed for naproxen and BPA ($k_{\text{ini}} = 0.45$ and 0.35 h^{-1} for naproxen and BPA, respectively) during 6 h of oxidative reaction. BPA has been considered as a well-known refractory pollutant that is not effectively

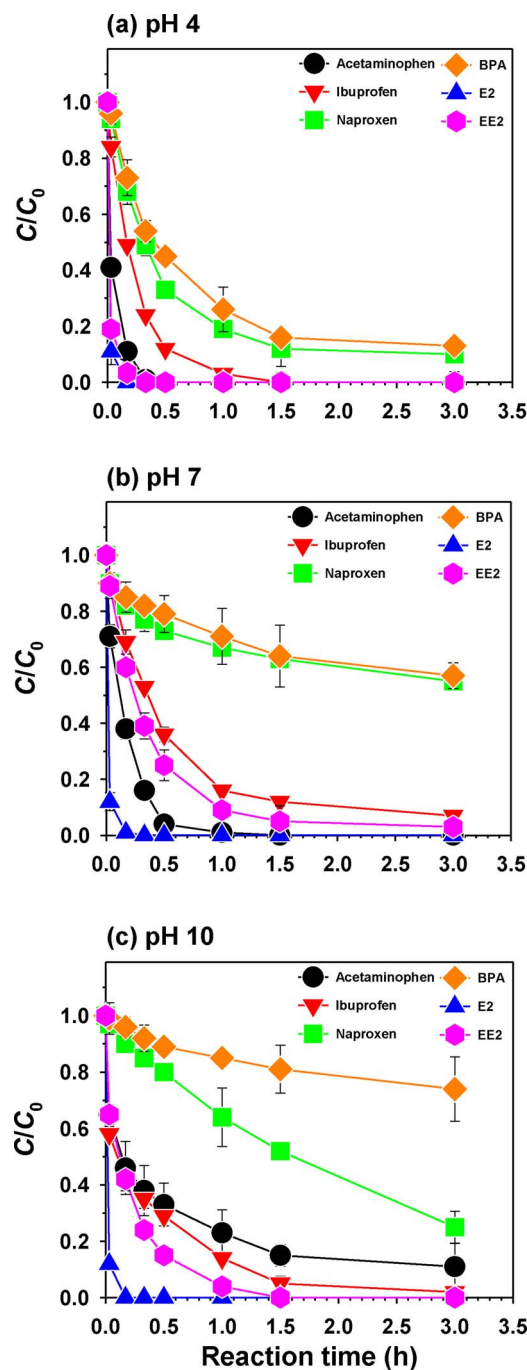


Fig. 6. Removal of acetaminophen, ibuprofen, naproxen, BPA, E2, and EE2 by rGO-Ag⁰/Fe₃O₄ NH in catalytic activation of PDS. Experimental conditions: [rGO-Ag⁰/Fe₃O₄]₀ = 0.1 g/L; [acetaminophen]₀ = [ibuprofen]₀ = [naproxen]₀ = [BPA]₀ = [E2]₀ = [EE2]₀ = 10 μM; [PDS]₀ = 1 mM; pH = 4, 7, and 10; and temperature = 298 K.

degraded in Fenton-like processes, even though the engineered NMs (e.g., AgNP and NZVI) are present under neutral/basic conditions [63]. The electro-oxidation of BPA generally requires a two-electron transfer process, which may retard the catalytic degradation of BPA [64].

Although the active SO₄^{·-} species tend to be rapidly quenched by Cl⁻ (used for pH adjustment) under acidic conditions [1,65], efficient degradation of the organic compounds were still achieved. This suggests that the non-radical oxidation may play a role in the PDS/rGO-Ag⁰/Fe₃O₄ system. In contrast, a higher substrate-dependent reactivity (i.e., a significant reduction in k_{ini} of naproxen and BPA) at higher pH values accounted for the reduced SO₄^{·-} resulted from radicals

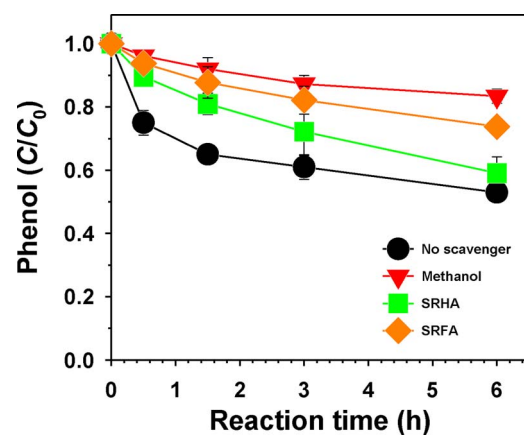


Fig. 7. Removal of phenol in PDS/GO-Ag⁰/Fe₃O₄ system in the presence of reactive oxidant scavenger [methanol and natural organic matter (SRHA and SRFA)]. Experimental conditions: [rGO-Ag⁰/Fe₃O₄]₀ = 0.1 g/L; [phenol]₀ = 10 μM; [PDS]₀ = 1 mM; [Methanol]₀ = 100 mM; [SRHA]₀ = [SRFA]₀ = 10 mg/L; pH = 7; and temperature = 298 K.

conversion into ·OH (Eq. (7)) in PDS/rGO-Ag⁰/Fe₃O₄ system. This indicates that SO₄^{·-} are considered as the dominant radical species apart from non-radical pathway and had a better selectivity toward naproxen and BPA under acidic conditions. To better identify the activities of oxidative degradation in catalytic removal of organic pollutants, the adsorption capacity of rGO-Ag⁰/Fe₃O₄ for various organic compounds and the scavenging effect on free radical species should be studied further at different pH values.

3.5. Mechanism of PDS activation by rGO-Ag⁰/Fe₃O₄ NH

Excess oxidant scavenger that may rapidly quench free SO₄^{·-} and ·OH in the aqueous suspension was used to shed light on the contribution of free reactive radicals to the oxidative degradation of phenol in a PDS/rGO-Ag⁰/Fe₃O₄ system (Fig. 7). Methanol was used for its SO₄^{·-} and ·OH scavenging activity, and SRHA and SRFA were used to test natural organic matter (NOM), rich in electrons, as a radical scavenger [66]. Methanol is a well-known oxidant scavenger that shows ~300 times less reactivity with SO₄^{·-} than ·OH [67]. Interestingly, the hydrophilic methanol (methanol:PDS molar ratio of 100:1) significantly decreased the oxidation efficiency (from 47% without scavengers to 17% with 100 mM of methanol) by dramatically scavenging free SO₄^{·-} and ·OH (> 80% of inhibition after 6 h of reaction) formed during the reaction under neutral conditions (pH 7). The catalytic phenol removal decreased, to 41 and 26% at pH 7, in the presence of 10 mg/L SRHA and SRFA, respectively. This indicates that SRHA and SRFA can also quench phenol degradation (12.8 and 44.7% of inhibition after 6 h of reaction, respectively) in a PDS/rGO-Ag⁰/Fe₃O₄ system due to the competing reactions of NOM with SO₄^{·-} and ·OH. Our previous study has shown that SRHA full of -COOH, -OH, and -NH₂ functional groups is weakly bound to rGO-Ag⁰/Fe₃O₄ NH [43]. This suggests that the higher amount of (free) SRHA remaining in suspension resulted in much less impact on radical scavenging activity. The competitive reactions of radical scavengers (methanol and NOM) with SO₄^{·-} and ·OH inhibited the removal efficiency for phenol, but partial degradation of phenol could still be achieved via a non-radical oxidative pathway or ·OH converted from SO₄^{·-}. However, further study is necessary to examine the type of oxidizing radical species involved or any non-radical oxidative pathway responsible for the degradation of phenol in PDS/rGO NH system. For example, *tert*-butyl alcohol (t-BuOH) may further inhibit the catalytic degradation via free ·OH formation [68]. The connected structure of rGO with Ag⁰ and Fe₃O₄ NPs may facilitate an electron transfer from phenol (electron donor) to PDS (electron acceptor), while rGO can serve as an electron-transfer

mediator [69].

4. Conclusions

rGO-Ag⁰/Fe₃O₄ NH was prepared by deposition of Ag⁰ and Fe₃O₄ NPs on rGO via *in situ* nucleation and crystallization. The NH showed a higher adsorption capacity of phenol than that of other single NPs (AgNP, NZVI, and rGO) at all pH values examined and could efficiently oxidize phenol in the heterogeneous activation of PDS. The catalytic performance of rGO-Ag⁰/Fe₃O₄ was higher under acidic conditions, and PDS/rGO-Ag⁰/Fe₃O₄ coupled process played a more dominant role in the oxidative degradation of phenol than H₂O₂/rGO-Ag⁰/Fe₃O₄ coupled process. The mechanistic study showed the synergistic effects between the adsorption and catalytic oxidation on NH for phenol removal. The enhanced performance of adsorption and oxidation of rGO-Ag⁰/Fe₃O₄ could be attributable to the incorporation of rGO with individual NPs (i.e., Ag⁰ and Fe₃O₄), promoting reactive sites for adsorption, catalytic oxidation, and electron transfer processes, oxidizing phenol via a non-radical oxidative pathway on the NH surface. Various organic pollutants were also tested to gain a better understanding of the selectivity of rGO-Ag⁰/Fe₃O₄ under different pH conditions. Promisingly, more than 99% of the acetaminophen and E2 were removed in PDS/rGO-Ag⁰/Fe₃O₄ system within 1 h of reaction at a neutral pH. As the solution pH increased, the reduced SO₄²⁻, due to recombination with ·OH, significantly decreased the removal efficiency of naproxen and BPA. This excellent magnetically-separable nanocatalyst may be a potential alternative in the oxidation of various organic compounds, preventing secondary pollution. Further research should be conducted to gain a better understanding of its reusability and possible degradation pathway of phenol prior to the practical application of this heterogeneous PDS/rGO-Ag⁰/Fe₃O₄ system.

Acknowledgments

This study was funded by the U.S. Environmental Protection Agency and the Korea Ministry of Environment, 'GAIA Project, 2015000540003'. This article has been reviewed in accordance with U.S. Environmental Protection Agency policy and approved for publication. However, the research results do not necessarily reflect the views or policies, and no official endorsement should be inferred.

Appendix A. Supplementary data

Supplementary data associated with this article can be found, in the online version, at <http://dx.doi.org/10.1016/j.apcatb.2017.11.058>.

References

- M.G. Antoniou, A. Armah, D.D. Dionysiou, Degradation of microcystin-LR using sulfate radicals generated through photolysis, thermolysis and e- transfer mechanisms, *Appl. Catal. B* 96 (2010) 290–298.
- P. Avetta, A. Pensato, M. Minella, M. Malandrino, V. Maurino, C. Minero, K. Hanna, D. Vione, Activation of persulfate by irradiated magnetite: implications for the degradation of phenol under heterogeneous photo-Fenton-like conditions, *Environ. Sci. Technol.* 49 (2014) 1043–1050.
- J. Zou, J. Ma, L. Chen, X. Li, Y. Guan, P. Xie, C. Pan, Rapid acceleration of ferrous iron/peroxymonosulfate oxidation of organic pollutants by promoting Fe (III)/Fe (II) cycle with hydroxylamine, *Environ. Sci. Technol.* 47 (2013) 11685–11691.
- T. Zeng, X. Zhang, S. Wang, H. Niu, Y. Cai, Spatial confinement of a Co3O4 catalyst in hollow metal-organic frameworks as a nanoreactor for improved degradation of organic pollutants, *Environ. Sci. Technol.* 49 (2015) 2350–2357.
- J. Deng, Y. Shao, N. Gao, Y. Deng, S. Zhou, X. Hu, Thermally activated persulfate (TAP) oxidation of antiepileptic drug carbamazepine in water, *Chem. Eng. J.* 228 (2013) 765–771.
- R. Hazime, Q. Nguyen, C. Ferronato, T. Huynh, F. Jaber, J.-M. Chovelon, Optimization of imazalil removal in the system UV/TiO2/K2S2O8 using a response surface methodology (RSM), *Appl. Catal. B* 132 (2013) 519–526.
- B. Li, L. Li, K. Lin, W. Zhang, S. Lu, Q. Luo, Removal of 1, 1, 1-trichloroethane from aqueous solution by a sono-activated persulfate process, *Ultrason. Sonochem.* 20 (2013) 855–863.
- N. Liu, G. Xu, M. Wu, X. He, L. Tang, W. Shi, L. Wang, H. Shao, Radical-induced destruction of diethyl phthalate in aqueous solution: kinetics, spectral properties, and degradation efficiencies studies, *Res. Chem. Intermed.* 39 (2013) 3727–3737.
- G.P. Anipsitakis, D.D. Dionysiou, Radical generation by the interaction of transition metals with common oxidants, *Environ. Sci. Technol.* 38 (2004) 3705–3712.
- C. Liang, Y.-Y. Guo, Y.-C. Chien, Y.-J. Wu, Oxidative degradation of MTBE by pyrite-activated persulfate: proposed reaction pathways, *Ind. Eng. Chem. Res.* 49 (2010) 8858–8864.
- J. Yan, M. Lei, L. Zhu, M.N. Anjum, J. Zou, H. Tang, Degradation of sulfamonomethoxine with Fe3O4 magnetic nanoparticles as heterogeneous activator of persulfate, *J. Hazard. Mater.* 186 (2011) 1398–1404.
- L. Zhu, Z. Ai, W. Ho, L. Zhang, Core-shell Fe-Fe2O3 nanostructures as effective persulfate activator for degradation of methyl orange, *Sep. Purif. Technol.* 108 (2013) 159–165.
- S. Bai, X. Shen, X. Zhong, Y. Liu, G. Zhu, X. Xu, K. Chen, One-pot solvothermal preparation of magnetic reduced graphene oxide-ferrite hybrids for organic dye removal, *Carbon* 50 (2012) 2337–2346.
- I. Hussain, Y. Zhang, S. Huang, X. Du, Degradation of p-chloroaniline by persulfate activated with zero-valent iron, *Chem. Eng. J.* 203 (2012) 269–276.
- A. Ghauch, G. Ayoub, S. Naim, Degradation of sulfamethoxazole by persulfate assisted micrometric FeO in aqueous solution, *Chem. Eng. J.* 228 (2013) 1168–1181.
- Y. Wang, R. Cheng, Z. Wen, L. Zhao, Synthesis and characterization of single-crystalline MnFe2O4 ferrite nanocrystals and their possible application in water treatment, *Eur. J. Inorg. Chem.* 2011 (2011) 2942–2947.
- H. Sun, C. Kwan, A. Suvorova, H.M. Ang, M.O. Tadé, S. Wang, Catalytic oxidation of organic pollutants on pristine and surface nitrogen-modified carbon nanotubes with sulfate radicals, *Appl. Catal. B* 154 (2014) 134–141.
- H. Lee, H.-J. Lee, J. Jeong, J. Lee, N.-B. Park, C. Lee, Activation of persulfates by carbon nanotubes: oxidation of organic compounds by nonradical mechanism, *Chem. Eng. J.* 266 (2015) 28–33.
- P. Shi, R. Su, S. Zhu, M. Zhu, D. Li, S. Xu, Supported cobalt oxide on graphene oxide: highly efficient catalysts for the removal of Orange II from water, *J. Hazard. Mater.* 229 (2012) 331–339.
- W. Peng, S. Liu, H. Sun, Y. Yao, L. Zhi, S. Wang, Synthesis of porous reduced graphene oxide as metal-free carbon for adsorption and catalytic oxidation of organics in water, *J. Mater. Chem. A* 1 (2013) 5854–5859.
- H. Sun, S. Liu, G. Zhou, H.M. Ang, M.O. Tadé, S. Wang, Reduced graphene oxide for catalytic oxidation of aqueous organic pollutants, *ACS Appl. Mater. Interfaces* 4 (2012) 5466–5471.
- R.K. Upadhyay, N. Soin, S.S. Roy, Role of graphene/metal oxide composites as photocatalysts, adsorbents and disinfectants in water treatment: a review, *RSC Adv.* 4 (2014) 3823–3851.
- Z. Wang, C. Xu, G. Gao, X. Li, Facile synthesis of well-dispersed Pd-graphene nanohybrids and their catalytic properties in 4-nitrophenol reduction, *RSC Adv.* 4 (2014) 13644–13651.
- Y. Yao, S. Miao, S. Liu, L.P. Ma, H. Sun, S. Wang, Synthesis, characterization, and adsorption properties of magnetic Fe3O4@graphene nanocomposite, *Chem. Eng. J.* 184 (2012) 326–332.
- S. Yang, W. Yue, J. Zhu, Y. Ren, X. Yang, Graphene-based mesoporous SnO₂ with enhanced electrochemical performance for lithium-ion batteries, *Adv. Funct. Mater.* 23 (2013) 3570–3576.
- E. Lee, J.-Y. Hong, H. Kang, J. Jang, Synthesis of TiO₂ nanorod-decorated graphene sheets and their highly efficient photocatalytic activities under visible-light irradiation, *J. Hazard. Mater.* 219 (2012) 13–18.
- A. Al-Anazi, W.H. Abdelraheem, C. Han, M.N. Nadagouda, L. Sygellou, M.K. Arfanis, P. Falaras, V.K. Sharma, D.D. Dionysiou, Cobalt ferrite nanoparticles with controlled composition-peroxymonosulfate mediated degradation of 2-phenylbenzimidazole-5-sulfonic acid, *Appl. Catal. B* 221 (2018) 266–279.
- G. Hu, B. Tang, Photocatalytic mechanism of graphene/titanate nanotubes photocatalyst under visible-light irradiation, *Mater. Chem. Phys.* 138 (2013) 608–614.
- D. Fu, G. Han, Y. Chang, J. Dong, The synthesis and properties of ZnO-graphene nano hybrid for photodegradation of organic pollutant in water, *Mater. Chem. Phys.* 132 (2012) 673–681.
- N. Yusoff, N. Huang, M. Muhamad, S. Kumar, H. Lim, I. Harrison, Hydrothermal synthesis of CuO/functionalized graphene nanocomposites for dye degradation, *Mater. Lett.* 93 (2013) 393–396.
- Z. Gao, J. Liu, F. Xu, D. Wu, Z. Wu, K. Jiang, One-pot synthesis of graphene-cuprous oxide composite with enhanced photocatalytic activity, *Solid State Sci.* 14 (2012) 276–280.
- Y. Fu, X. Wang, Magnetically separable ZnFe2O4-graphene catalyst and its high photocatalytic performance under visible light irradiation, *Ind. Eng. Chem. Res.* 50 (2011) 7210–7218.
- J. Xia, J. Di, S. Yin, H. Xu, J. Zhang, Y. Xu, L. Xu, H. Li, M. Ji, Facile fabrication of the visible-light-driven Bi2WO6/BiOBr composite with enhanced photocatalytic activity, *RSC Adv.* 4 (2014) 82–90.
- Y. Yao, C. Xu, S. Yu, D. Zhang, S. Wang, Facile synthesis of Mn3O4-reduced graphene oxide hybrids for catalytic decomposition of aqueous organics, *Ind. Eng. Chem. Res.* 52 (2013) 3637–3645.
- Y. Yao, Z. Yang, H. Sun, S. Wang, Hydrothermal synthesis of Co3O4-graphene for heterogeneous activation of peroxymonosulfate for decomposition of phenol, *Ind. Eng. Chem. Res.* 51 (2012) 14958–14965.
- Y. Yao, C. Xu, S. Miao, H. Sun, S. Wang, One-pot hydrothermal synthesis of Co(OH)₂ nanoflakes on graphene sheets and their fast catalytic oxidation of phenol in liquid phase, *J. Colloid Interface Sci.* 402 (2013) 230–236.
- Y. Yao, Y. Cai, F. Lu, F. Wei, X. Wang, S. Wang, Magnetic recoverable MnFe2O4 and MnFe2O4-graphene hybrid as heterogeneous catalysts of peroxymonosulfate activation for efficient degradation of aqueous organic pollutants, *J. Hazard. Mater.*

270 (2014) 61–70.

[38] Y. Yao, Z. Yang, D. Zhang, W. Peng, H. Sun, S. Wang, Magnetic CoFe2O4–graphene hybrids: facile synthesis, characterization, and catalytic properties, *Ind. Eng. Chem. Res.* 51 (2012) 6044–6051.

[39] J.M. Conley, S.J. Symes, M.S. Schorr, S.M. Richards, Spatial and temporal analysis of pharmaceutical concentrations in the upper Tennessee River basin, *Chemosphere* 73 (2008) 1178–1187.

[40] E. Godfrey, W.W. Woessner, M.J. Benotti, Pharmaceuticals in on-site sewage effluent and ground water, *Western Montana: Ground Water* 45 (2007) 263–271.

[41] M.J. Benotti, R.A. Trenholm, B.J. Vanderford, J.C. Holady, B.D. Stanford, S.A. Snyder, Pharmaceuticals and endocrine disrupting compounds in US drinking water, *Environ. Sci. Technol.* 43 (2008) 597–603.

[42] R. Shen, S.A. Andrews, Demonstration of 20 pharmaceuticals and personal care products (PPCPs) as nitrosamine precursors during chloramine disinfection, *Water Res.* 45 (2011) 944–952.

[43] C.M. Park, D. Wang, J. Heo, N. Her, C. Su, Aggregation of reduced graphene oxide and its nano-hybrids with magnetite and elemental silver under environmentally relevant conditions, *Sci. Total Environ.* (2017) (underreview).

[44] C. Chen, Q.H. Yang, Y. Yang, W. Lv, Y. Wen, P.X. Hou, M. Wang, H.M. Cheng, Self-assembled free-standing graphite oxide membrane, *Adv. Mater.* 21 (2009) 3007–3011.

[45] V.R. Bari, U. Dhorda, M. Sundaresan, A simultaneous packed column supercritical fluid chromatographic method for ibuprofen, chlorzoxazone and acetaminophen in bulk and dosage forms, *Talanta* 45 (1997) 297–302.

[46] S. Stankovich, D.A. Dikin, G.H. Dommett, K.M. Kohlhaas, E.J. Zimney, E.A. Stach, R.D. Piner, S.T. Nguyen, R.S. Ruoff, Graphene-based composite materials, *Nature* 442 (2006) 282–286.

[47] W. Liu, J. Ma, C. Shen, Y. Wen, W. Liu, A pH-responsive and magnetically separable dynamic system for efficient removal of highly dilute antibiotics in water, *Water Res.* 90 (2016) 24–33.

[48] R. Bandyopadhyay, J. Selbo, G.E. Amidon, M. Hawley, Application of powder X-ray diffraction in studying the compaction behavior of bulk pharmaceutical powders, *J. Pharm. Sci.* 94 (2005) 2520–2530.

[49] H. Yang, R. Yan, H. Chen, D.H. Lee, C. Zheng, Characteristics of hemicellulose, cellulose and lignin pyrolysis, *Fuel* 86 (2007) 1781–1788.

[50] S.-T. Yang, Y. Chang, H. Wang, G. Liu, S. Chen, Y. Wang, Y. Liu, A. Cao, Folding/aggregation of graphene oxide and its application in Cu²⁺ removal, *J. Colloid Interface Sci.* 351 (2010) 122–127.

[51] G.E. Hoag, J.B. Collins, J.L. Holcomb, J.R. Hoag, M.N. Nadagouda, R.S. Varma, Degradation of bromothymol blue by 'greener' nano-scale zero-valent iron synthesized using tea polyphenols, *J. Mater. Chem.* 19 (2009) 8671–8677.

[52] B. Mahitha, B.D.P. Raju, G. Dillip, C.M. Reddy, K. Mallikarjuna, L. Manoj, S. Priyanka, K.J. Rao, N.J. Sushma, Biosynthesis, characterization and antimicrobial studies of AgNPs extract from Bacopa monniera whole plant, *Dig. J. Nanomat. Biostruct.* 6 (2011) 135–142.

[53] T. Hartono, S. Wang, Q. Ma, Z. Zhu, Layer structured graphite oxide as a novel adsorbent for humic acid removal from aqueous solution, *J. Colloid Interface Sci.* 333 (2009) 114–119.

[54] Y. Heo, H. Im, J. Kim, The effect of sulfonated graphene oxide on sulfonated poly (ether ketone) membrane for direct methanol fuel cells, *J. Membr. Sci.* 425 (2013) 11–22.

[55] P. Jiang, S.Y. Li, S.S. Xie, Y. Gao, L. Song, Machinable long PVP-stabilized silver nanowires, *Chem. Eur. J.* 10 (2004) 4817–4821.

[56] R. Singh, A. Samariya, S. Kumar, S. Sharma, Y. Xing, U. Deshpande, T. Shripati, E. Saitovitch, A close correlation between induced ferromagnetism and oxygen deficiency in Fe doped In2O3, *Appl. Surf. Sci.* 257 (2010) 1053–1057.

[57] C. Qi, X. Liu, J. Ma, C. Lin, X. Li, H. Zhang, Activation of peroxyomonosulfate by base: implications for the degradation of organic pollutants, *Chemosphere* 151 (2016) 280–288.

[58] C. Liang, H.-W. Su, Identification of sulfate and hydroxyl radicals in thermally activated persulfate, *Ind. Eng. Chem. Res.* 48 (2009) 5558–5562.

[59] S.A. Mokhtari, M. Farzadkia, A. Esrafil, R.R. Kalantari, A.J. Jafari, M. Kermani, M. Gholami, Bisphenol A removal from aqueous solutions using novel UV/persulfate/H2O2/Cu system: optimization and modelling with central composite design and response surface methodology, *J. Environ. Health Sci. Eng.* 14 (2016) 19.

[60] Y.-S. Ho, G. McKay, Pseudo-second order model for sorption processes, *Process Biochem.* 34 (1999) 451–465.

[61] C.M. Park, J. Han, K.H. Chu, Y.A. Al-Hamadani, N. Her, J. Heo, Y. Yoon, Influence of solution pH, ionic strength, and humic acid on cadmium adsorption onto activated biochar: experiment and modeling, *J. Ind. Eng. Chem.* 48 (2017) 186–193.

[62] X. Wang, S. Huang, L. Zhu, X. Tian, S. Li, H. Tang, Correlation between the adsorption ability and reduction degree of graphene oxide and tuning of adsorption of phenolic compounds, *Carbon* 69 (2014) 101–112.

[63] C.M. Park, J. Heo, Y. Yoon, Oxidative degradation of bisphenol A and 17 α -ethinyl estradiol by Fenton-like activity of silver nanoparticles in aqueous solution, *Chemosphere* 168 (2017) 617–622.

[64] B. Ntsendwana, B. Mamba, S. Sampath, O. Arotiba, Electrochemical detection of bisphenol A using graphene-modified glassy carbon electrode, *Int. J. Electrochem. Sci.* 7 (2012) 3501–3512.

[65] X. Duan, Z. Ao, L. Zhou, H. Sun, G. Wang, S. Wang, Occurrence of radical and nonradical pathways from carbocatalysts for aqueous and nonaqueous catalytic oxidation, *Appl. Catal. B* 188 (2016) 98–105.

[66] C.R. Keenan, D.L. Sedlak, Factors affecting the yield of oxidants from the reaction of nanoparticulate zero-valent iron and oxygen, *Environ. Sci. Technol.* 42 (2008) 1262–1267.

[67] J.A. Khan, X. He, N.S. Shah, H.M. Khan, E. Hapeshi, D. Fatta-Kassinos, D.D. Dionysiou, Kinetic and mechanism investigation on the photochemical degradation of atrazine with activated H2O2, S2O82–, and HSO5–, *Chem. Eng. J.* 252 (2014) 393–403.

[68] X. He, A. Armah, K.E. O'Shea, D.D. Dionysiou, Kinetics and mechanisms of cylindrospermopsin destruction by sulfate radical-based advanced oxidation processes, *Water Res.* 63 (2014) 168–178.

[69] D. Li, X. Duan, H. Sun, J. Kang, H. Zhang, M.O. Tade, S. Wang, Facile synthesis of nitrogen-doped graphene via low-temperature pyrolysis: the effects of precursors and annealing ambience on metal-free catalytic oxidation, *Carbon* 115 (2017) 649–658.